JACS
JOURNAL OF THE AMERICAN CHEMICAL SOCIETY
Article
pubs.acs.org/JACS

Tuning the Size and Properties of ClyA Nanopores Assisted by Directed Evolution

Misha Soskine, Annemie Biesemans, Marc De Maeyer, and Giovanni Maglia*

Department of Chemistry, University of Leuven, Leuven, 3001, Belgium

Supporting Information

ABSTRACT: Nanopores have recently emerged as powerful tools in single-molecule investigations. Biological nanopores, however, have drawbacks, including a fixed size and limited stability in lipid bilayers. Inspired by the great success of directed evolution approaches in tailoring enzyme properties, in this work we evolved Cytolysin A from *Salmonella typhi* (ClyA) to a high level of soluble expression and desired electrical properties in lipid bilayers. Evolved ClyA nanopores remained open up to −150 mV applied potential, which allowed the detailed characterization of folded proteins by ionic current recordings. Remarkably, we also found that ClyA forms several nanopore species; among which we could isolate and characterize three nanopore types most likely corresponding to the 12mer, 13mer, and 14mer oligomeric forms of ClyA. Protein current blockades to the three ClyA nanopores showed that subnanometer variations in the diameter of nanopores greatly affect the recognition of analyte proteins.

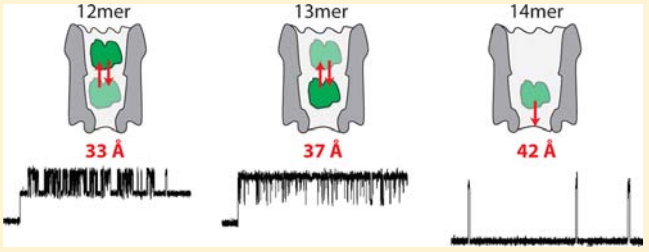

INTRODUCTION

The transport of ions or molecules across a biological membrane is a fundamental process in cellular life and is tightly regulated by ion channels, transporters, and pores. Recently, researchers have adopted biological,[1−3] solid-state,[4,5] glass,[6,7] DNA origami[8−11] and hybrid[12] nanopores in single-molecule analysis.[13] Biological nanopores have advantages compared to their synthetic counterparts, mostly because they can be reproducibly fabricated and modified with an atomic level precision that cannot yet be matched by artificial nanopores. Biological nanopores, however, also have drawbacks. The mechanical stability of biological nanopores depends on individual cases. Several biological nanopores remain open in lipid bilayers at high applied potentials and can cope surprisingly well with extreme conditions of temperature,[14,15] pH,[15−18] and denaturant concentrations.[15,18−20] However, other porins and channels are much less robust. Arguably, still, the greatest disadvantage of biological nanopores is their limited repertoire of possible sizes.

A significant number of studies sampled the translocation of proteins through artificial nanopores.[21−27] Nonetheless, the investigation of proteins with solid-state nanopores is difficult because proteins have a nonuniform charge distribution, they often adsorb to the nanopore surface, and they translocate too quickly to be properly sampled.[28] Furthermore, because proteins have a compact folded structure, the diameter of the nanopore should be similar to that of the protein.[22] Biological nanopores have also been used to characterize proteins. However, the small internal diameter (∼1 nm) of the most common nanopores such as αHL, MspA, or aerolysin, although they allowed the analysis of small peptides or unfolded proteins,[29−38] precludes the direct investigations of folded proteins. Among the larger biological nanopores, the connector protein in the bacteriophage phi29 DNA-packaging motor has been modified to insert into artificial bilayers to form nanopores of ∼3.5 nm diameter (phi29 nanopores).[39] Despite their suitable size, however, phi29 nanopores have not yet been used to investigate proteins. More recently, bacterial ferric hydroxamate uptake component A (FhuA) has been engineered to produce a stable nanopore, the open pore ionic current of which can be transiently blocked by folded protein analytes.[40]

Recently, we have introduced Cytolysin A from *Salmonella typhi* (ClyA) as the first biological nanopore that allows the accommodation of natively folded proteins within the nanopore lumen.[41] The ClyA structure is ideal for analyzing proteins because proteins such as thrombin (37 kDa) or malate dehydrogenase (dimer, 35 kDa monomer)[41] can be electrophoretically trapped between the wide cis entrance and the narrower trans exit of the pore, and can therefore be sampled for several minutes. Ionic currents through ClyA are so sensitive to the vestibule environment that blockades of human and bovine thrombins can be easily distinguished.[41] Our work was based on a ClyA construct where the two native cysteine residues (Cys87 and Cys285) of ClyA wild type (ClyA-WT) were replaced by serine (ClyA-SS, where the SS suffix indicates the two serine amino acids replacing the cysteine residues in the native sequence) so that an additional cysteine residue could be incorporated and chemically modified at the nanopore

Received: May 28, 2013
Published: August 6, 2013

   dx.doi.org/10.1021/ja4053398 | J. Am. Chem. Soc. 2013, 135, 13456−13463

surface.[41] ClyA nanopores, however, showed several drawbacks. ClyA-WT displayed a heterogeneous unitary conductance distribution and ClyA-WT and ClyA-SS monomers mostly expressed in inclusion bodies (see below). Further, ClyA-SS monomers showed low water solubility and poor hemolytic activity (Supporting Information, SI, Figure S1). Finally, in planar lipid bilayers ClyA-SS spontaneously opened and closed (gated) at applied potentials higher than +60 mV or lower than −90 mV.[41] Therefore, we aimed to obtain a ClyA variant amenable to site−specific chemical modifications (not including cysteine residues) with desired properties of solubility, activity, and stability in planar lipid bilayers.

RESULTS AND DISCUSSION

Tuning the Properties of ClyA by Directed Evolution. Inspired by the great success of directed evolution approaches in tailoring enzymes with desired properties, we used directed evolution to improve the activity of ClyA-SS, reasoning that mutations compensating for the deleterious effects of C87S and C285S substitutions would also increase the soluble expression and stability of ClyA. Random libraries were generated on the background of ClyA-SS by error prone PCR (approximately 1−4 mutations per gene per round) and screened for hemolytic activity (SI Figure S1). The most active variants were then purified by Ni-NTA affinity chromatography and tested for oligomer formation by blue native polyacrylamide gel electrophoresis (BN-PAGE, SI Figure S2). Selected nanopore variants were finally screened in planar lipid bilayers for the desired behavior (uniformity of formed channels, low electrical noise, and ability to remain open at high applied potentials), which served as final and critical criteria for selection. After just four rounds of screening, we isolated ClyA-CS variant (Figure 1 and Table 1) that showed low electrical noise and remained open in planar lipid bilayers from +90 mV to −150 mV (SI Figure S3). ClyA-CS displayed five mutations relative to the ClyA-SS sequence: S87C, L99Q, E103G, F166Y, and K294R (Figure 1). All of the accumulated mutations correspond to positions that are located outside the lumen of the nanopore according to the *E. coli* ClyA crystal structure[42] (Figure 1) and do not have an obvious role in the stability or hemolytic activity of the nanopore; with the only possible exception of phenylalanine 166, which is located next to the cluster of hydrophobic residues implicated in the prepore to pore transition of ClyA.[42] Remarkably, the serine at position 87 converted back to cysteine, the original residue in the wild-type gene (Figure 1). Since we desired to obtain a cysteine-less ClyA variant amenable to site-specific chemical modification, we subjected ClyA-CS to an additional round of directed evolution (additional results in the SI), from which we selected ClyA-AS with desired electrical properties. In ClyA-AS, cysteine 87 was converted to alanine and isoleucine 203 to valine (Figure 1), the latter being the same residue as in *E. coli* ClyA-WT. Contrary to ClyA-SS and ClyA-WT, evolved ClyA variants expressed in *E. coli* cells in the soluble fraction (SI Figure S1) and could be purified without the use of detergents, allowing a ∼10-fold increase in the purification yield (∼0.6 mg pure ClyA-CS per 10 mL culture).

Isolation of ClyA Nanopores with Different Conductance. ClyA-WT, ClyA-SS, and evolved ClyA oligomers, formed by incubation of purified ClyA monomers with 0.5% w/v β-dodecyl maltoside (DDM), migrated as multiple, closely spaced bands on a blue native gradient PAGE (Figure 2a). In lipid bilayers, ClyA nanopores reconstitute with a preferred

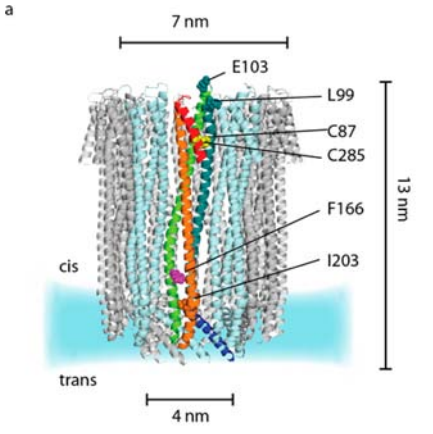

b

Round	Name	Sequence changes
0	ClyA-SS	C87S, C285S
4	ClyA-CS	L99Q, E103G, F166Y, C285S, K294R
5	ClyA-AS	C87A, L99Q, E103G, F166Y, I203V, C285S, K294R, H307Y

Figure 1. Engineered ClyA nanopores. (a) Ribbon representation of a *S. typhi* ClyA nanopore, constructed by homology modeling from the *E. coli* ClyA structure (PDB: 2WCD, 90% sequence identity), displaying the amino acids side chains changed by the directed evolution experiments (displayed as spheres).[42] One protomer is highlighted, with the secondary structure elements colored from blue to red from N to C termini; other protomers are shown alternating in pale blue and gray. The two native cysteine residues are colored in yellow, while Phenylalanine 166 is colored in magenta. K294 and H307 are not displayed because they are not shown in the ClyA crystal structure. (b) Sequence changes in ClyA-SS, ClyA-CS, and ClyA-AS relative to ClyA-WT.

orientation (Figure 1) that can be assessed by the slightly asymmetrical current−voltage relationship of the pore.[41] Preassembled ClyA-WT nanopores showed a wide distribution of open nanopore conductance (G_O), spanning approximately 2 nS (Figure 2b, top and ref 43). The major peak in the distribution of unitary conductance corresponded to nanopores with an average conductance of 1.81 ± 0.04 nS (mean ± s.d.) that we named Type I (G_O range from 1.7 to 1.9 nS, at −35 mV, 15 mM Tris·HCl pH 7.5 and 150 mM NaCl, Table 1 and Figure 2b, top). Interestingly, evolved ClyA nanopores showed an altered pattern of conductance distributions. Preassembled ClyA-CS showed two major peaks: the first corresponded to Type I (1.79 ± 0.05 nS, mean ± s.d.), the second to a novel nanopore type with an average conductance of 2.23 ± 0.08 nS (mean ± s.d.) that we named Type II (G_O range from 2.1 to 2.4 nS, −35 mV, Table 1 and Figure 2b, middle). By contrast, ClyA-AS showed a relatively uniform distribution of mainly Type I nanopores (G_O = 1.80 ± 0.05, mean ± s.d., −35 mV, Figure 2b, bottom).

To establish whether the ClyA species with different electrophoretic mobility on BN-PAGE formed nanopores with different conductance, we gel-extracted ClyA-CS from the three lowest oligomeric bands and measured the unitary conductance of 62 nanopores at −35 mV derived from each band within two days from gel extraction. Remarkably, the majority of ClyA-CS oligomers from the lowest band (band 1) formed Type I ClyA-CS nanopores (1.79 ± 0.04 nS, mean ± s.d., Figure 3, top), while most of the nanopores extracted from the second lowest band (band 2) reconstituted as Type II

dx.doi.org/10.1021/ja4053398 | J. Am. Chem. Soc. 2013, 135, 13456−13463

Table 1. Parameters for ClyA-SS and ClyA-CS Nanopores[a]

	Type I ClyA-SS[b]	Type I ClyA-CS	Type II ClyA-CS	Type III ClyA-CS
trans diameter, nm	3.3	3.3	3.7	4.2
cis diameter, nm	5.5	5.5	5.9	6.5
G_O at −35 mV, nS	1.8 ± 0.1	1.79 ± 0.04	2.21 ± 0.08	2.64 ± 0.08
G_O at +35 mV, nS	2.0 ± 0.1	2.03 ± 0.20	2.42 ± 0.16	2.88 ± 0.08
G_O from eq 2	2.06	2.06	2.47	3.07
HT occupancy of L2 at −35 mV, %	22 ± 5	30 ± 10	96 ± 2	100 ± 0
HT level 1 at −35 mV, I_{RES}%	56 ± 1	56 ± 1	68 ± 1	NA
HT level 2 at −35 mV, I_{RES}%	23 ± 1	23 ± 3	31 ± 1	32 ± 9
HT occupancy of L2 at −150 mV, %	NA	100	100	NA
HT level 2 at −150 mV, I_{RES}, %	NA	23 ± 1	29 ± 2	NA
HT dwell time at −150 mV, ms	NA	172 ± 108	0.8 ± 0.4	NA

[a]The diameters of Type I ClyA-SS and ClyA-CS were taken from the crystal structure of *E. coli* ClyA (PDB: 2WCD). The diameters of Type II and Type III ClyA-CS were measured from the models shown in Figure 4d. The diameters were determined including the van der Waals radii of the atoms. The values of G_O are from the gel purified ClyA nanopores (Figure 3). Errors are given as standard deviations. [b]Data taken from ref 41.

ClyA-CS nanopores (G_O = 2.21 ± 0.08 nS, mean ± s.d., Figure 3, middle). Interestingly, a large fraction of the nanopores extracted from the third lowest band (band 3) reconstituted in lipid bilayers as a third nanopore type showing an average conductance of 2.64 ± 0.08 nS (mean ± s.d.) that we named Type III (G_O range from 2.5 to 3.0 nS, at −35 mV, Table 1, and Figure 3, bottom). In order to check whether the oligomers remained intact after gel purification, extracted ClyA oligomers were reloaded on a BN-PAGE. Despite the presence of faint additional bands probably originating from contamination during gel extraction and/or reversible oligomer to monomer transitions, gel purified Type I and Type II ClyA-CS oligomers migrated mainly as single bands, indicating that the nanopores remained largely intact after gel purification (SI Figure S2c,d).

These findings show that the three major ClyA bands observed on the BN-PAGE correspond to three distinct nanopore types. Although alternative folded ClyA structures cannot be excluded, the observation that ClyA oligomers with a slower electrophoretic migration form nanopores with higher conductance in lipid bilayers suggests that the three ClyA types might correspond to oligomers with different subunit stoichiometry. This is not necessarily surprising given that high order symmetrical oligomeric structures are often permissive with respect to subunit stoichiometry.[44−46] Interestingly, in a very recent study, the removal of a secondary structural element from a phi29 DNA-packaging motor produced nanopores with two different conductance levels that have been postulated to reflect nanopores with different oligomeric states.[47] Further, the exact stoichiometry of *E. coli* ClyA (~90% sequence identity to *Salmonella typhi* ClyA) oligomerization is controversial: the crystal structure (PDB_ID: 2WCD) revealed a dodecamer,[42] while earlier cryo-EM studies revealed nanopores with 8[48] or 13[49] subunits. Therefore, we hypothesize that the major band on the BN-PAGE corresponding to Type I ClyA most likely represents the 12mer of the crystal structure, while the band corresponding to Type II ClyA might be the 13mer observed in earlier cryo-EM studies. By analogy, Type III ClyA-CS nanopores may correspond to a 14mer version of ClyA not observed before. Both Type I and Type II ClyA-CS nanopores remained open at high negative-applied potentials (Figure 4a,b) and showed low electrical noise (Figure 4c). Type III ClyA-CS, however, was not very stable in lipid bilayers as shown by frequent gating events especially at applied potentials lower than −40 mV and higher than +50 mV. In addition, Type III ClyA-CS showed relatively high low-frequency noise (Figure 4c) and often gated irreversibly, (SI Figure S3b) precluding a routine use in planar lipid bilayers.

Molecular Models of the Three Type ClyA Nanopores. We prepared molecular models of the 13mer and 14mer ClyA nanopores by adding, respectively, one and two subunits to the 12mer of the *E. coli* ClyA crystal structure (Figure 4d) as described in the SI. The resistance R of a cylindrical nanopore with no surface charge (or where it plays no role) is often estimated from its length (l) and cross-section area (A) using the following expression:[50]

$$R = \frac{l}{A\sigma} \tag{1}$$

where σ is the bulk conductivity (1.59 S m^{-1} at 25 °C for 150 mM NaCl[51]). The lumen of ClyA nanopores can be simplified by two communicating cylinders: one that opens to the cis side (cis vestibule) and the other that opens to the trans side (trans vestibule or transmembrane region, Figure 4d). Therefore, as for resistors in series, the theoretical conductance of the three ClyA nanopore types can be calculated from the inverse of the sum of the resistance of the trans and cis vestibules by the following:

$$R_{ClyA} = \frac{4}{\sigma\pi}\left(\frac{l_{trans}}{d_{trans}^2} + \frac{l_{cis}}{d_{cis}^2}\right) \tag{2}$$

where l_{trans} is the length (3.0 nm) of the transmembrane region and d_{trans} its diameter (3.3, 3.7, and 4.2 nm for the 12mer, 13mer, and 14mer ClyA oligomers, respectively); and l_{cis} is the length (10.0 nm) and d_{cis} the diameter (5.5, 5.9, and 6.5 nm for the 12mer, 13mer, and 14mer ClyA, respectively) of the cis vestibule (Figure 4d and Table 1). From eq 2 the 12mer, 13mer, and 14mer ClyA pores have a theoretical open pore conductance ($G_{ClyA} = 1/R_{ClyA}$) of 2.06, 2.47, and 3.07 nS, respectively, which compare well to the G_O values measured at +35 mV for Type I, II, and III pores (2.03 ± 0.20, 2.42 ± 0.16, and 2.88 ± 0.08 nS, respectively, in 15 mM Tris.HCl pH 7.5 and 150 mM NaCl); and they were 14%, 11%, and 14% higher, respectively, than the G_O values at −35 mV (Table 1, Figure 4d). Therefore, although the calculated conductance values are only simple estimates, these results are compatible with our view that the three types of ClyA nanopores correspond to three pores with different oligomer composition.

Thrombin as Molecular Caliper to Test ClyA Nanopores of Different Size. We have previously shown that at

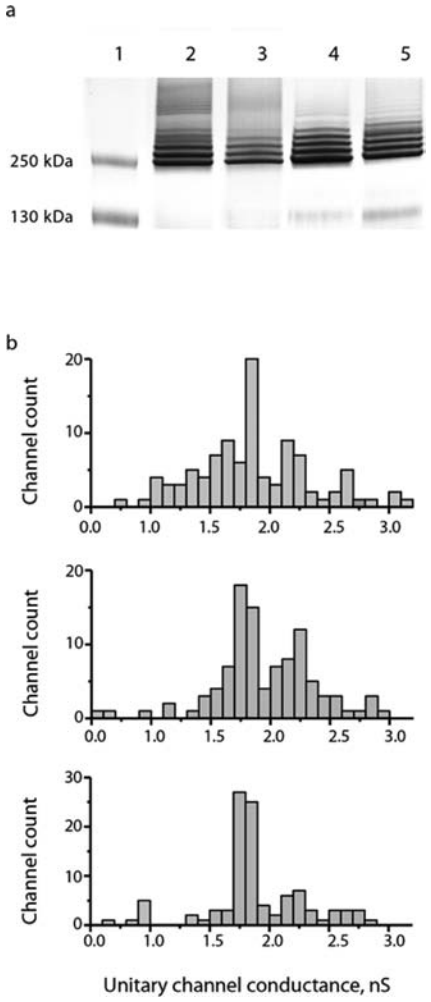

Figure 2. Oligomerization pattern and nanopore conductance of preoligomerized ClyA nanopores. (a) Oligomerization of ClyA nanopores examined by a 4−20% BN-PAGE. Proteins (1 mg/mL) were preincubated with 0.5% DDM for 30 min at 37 °C before loading into the gel (40 μg/lane). Lane 1: Protein ladder; lane 2: ClyA-WT; lane 3: ClyA-SS; lane 4: ClyA-AS; and lane 5: ClyA-CS. (b) Unitary nanopore conductance distribution obtained from 100 nanopores reconstituted in planar lipid bilayers for ClyA-WT (top), ClyA-CS (middle) and ClyA-AS (bottom) nanopores after preoligomerization in 0.5% DDM. Top: Type I ClyA-WT (G_O = 1.81 ± 0.04 nS, G_O range from 1.7 to 1.9 nS) and Type II ClyA-WT (G_O = 2.21 ± 0.07 nS, G_O range from 2.1 to 2.4 nS) represented 24% and 19% of the inserted nanopores, respectively. Middle: ClyA-CS open pore conductance showed two main peaks. Type I ClyA-CS (G_O = 1.79 ± 0.05 nS) included 35% and Type II ClyA-CS (2.23 ± 0.08 nS) 23% of the reconstituted nanopores. Bottom: the nanopore conductance of ClyA-AS was relatively uniform, with 52% of the reconstituted nanopores corresponding to Type I ClyA-AS (G_O = 1.80 ± 0.05 nS) and 16% to Type II ClyA-AS (G_O = 2.24 ± 0.09 nS). Recordings were carried out at −35 mV in 15 mM Tris·HCl, pH 7.5, 150 mM NaCl and the temperature was 28 °C. The errors represent the standard deviation of the mean.

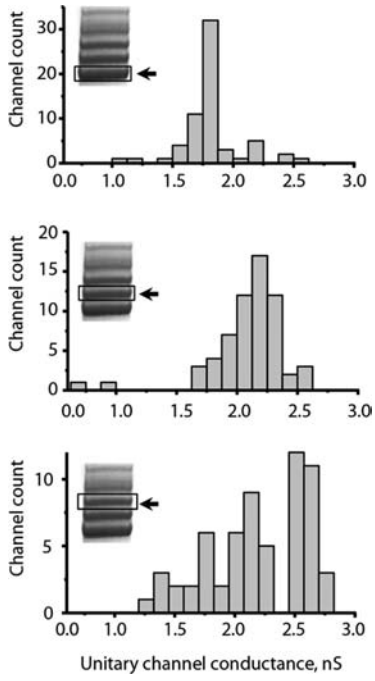

Figure 3. Isolation of different ClyA Types. Unitary conductance of 62 ClyA-CS nanopores extracted from the lowest (top), second lowest (middle) and third lowest (bottom) oligomeric band of ClyA-CS separated on 4−20% acrylamide BN-PAGE. The bands that were excized are boxed and marked with an arrow on the insets. Recordings were carried out at −35 mV, 28 °C in 15 mM Tris.HCl, pH 7.5 containing 150 mM NaCl. ClyA oligomers were extracted in 15 mM Tris·HCl pH 7.5, 150 mM NaCl containing 1 mM EDTA and 0.2% DDM.

−35 mV HT (human thrombin, 37 kDa) inflicted well-defined current blockades to Type I ClyA nanopores that lasted for several minutes due to the entry of HT into the lumen of the pore (Figure 5a, Table 1, SI Figure S3).[41] The current blockades switched rapidly between two blocked current levels: Level 1 [percentage of the open nanopore current ($I_{RES\%}$) = 56 ± 1%, mean ± s.d.] and level 2 ($I_{RES\%}$ = 23 ± 1%, mean ± s.d., Table 1, and Figure 5a). The current blockades were interpreted as HT occupying two residence sites (R1 and R2) within the lumen of the ClyA nanopore; where level 2 is most likely associated to HT residence at a deep more sterically constrained site R2, and level 1 is associated to the residence of HT at a site R1 located closer to the cis entrance of the nanopore (Figure 5a).[41] Because thrombin provoked such well-defined pattern of current blockades we chose HT as a molecular caliper to compare the geometries of the different types of ClyA nanopores.

At −35 mV, HT current blockades to Type I ClyA-CS nanopores were almost identical to that of Type I ClyA-SS nanopores (Table 1, Figure 5a, SI Figure S3c), confirming that mutations accumulated in the ClyA variants most likely did not change the size and geometry of the ClyA nanopore. HT current blockades to Type II ClyA also lasted for minutes (SI Figure S3) and switched between the two different current levels (Table 1, Figure 5a). In Type I ClyA-CS, however, HT mostly lodged at the more superficial R1 site (70% occupancy), while in Type II ClyA-CS HT preferred the deeper site R2 (96% occupancy, Table 1, Figure 5a). HT occupancy of R2 in Type II ClyA at −35 mV was the same as HT occupancy of R2 in Type I ClyA at −60 mV,[41] indicating that HT requires a higher driving force to populate the sterically constrained R2 site in Type I ClyA-CS. Interestingly, HT blockades to Type III ClyA-CS were fast (55 ± 48 ms) and showed only a level 2 current block ($I_{RES\%}$ = 32 ± 9%, mean ± s.d., Table 1, Figure 5a), suggesting an unhindered access to the R2 site at this potential. These results further support our hypothesis that the

dx.doi.org/10.1021/ja4053398 | J. Am. Chem. Soc. 2013, 135, 13456−13463

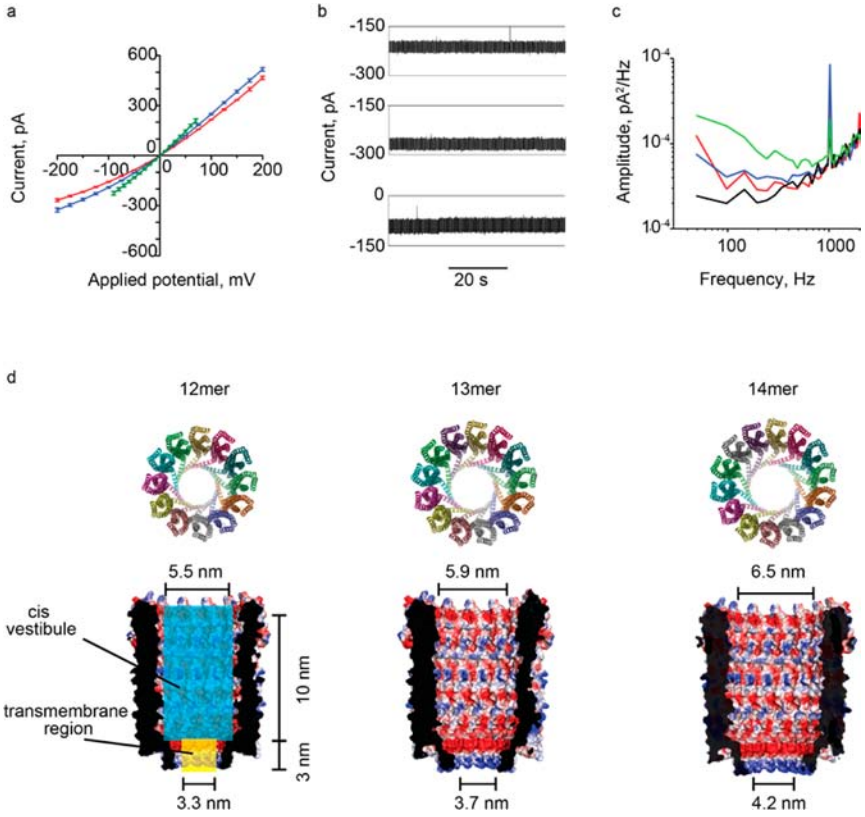

Figure 4. The three ClyA-CS nanopores. (a) Current−voltage (I−V) curves of Type I (red), Type II (blue), and Type III (green) ClyA-CS pores. The I−V curve of Type III ClyA-CS shows ionic currents sampled at potentials lower than ±100 mV due to the instability of the pore at higher applied potentials. (b) Ionic current recordings of Type I (top) and Type II (middle) ClyA-CS at −150 mV and Type III ClyA-CS (bottom) at −35 mV. (c) Current power spectral densities of the Type I (red), Type II (blue), and Type III (green) ClyA-CS nanopores at −35 mV obtained from 0.5 s traces showing the low frequency noise in ClyA-CS nanopores. The current power spectral density at 0 mV is shown in black. Each line corresponds to the average of power spectra calculated from 3 recordings carried out on different single channels. (d) Cartoon representation (top view, top) and surface representation (section through the side view, bottom) of the molecular models corresponding to the 12mer, 13mer, and 14mer *E. coli* ClyA nanopores. Each monomer in the cartoon representation is displayed with a different color (Pymol). Proteins in surface representations are colored according to their "in vacuum" electrostatics (red for negative regions and blue for positive regions, Pymol). The blue and yellow boxes (left section through) describe the theoretical cylinders corresponding to the cis vestibule and transmembrane region (trans vestibule), respectively, that are used to model the conductance of ClyA in eq 2. The diameters of the regions of the pores were determined including the van der Waals radii of the atoms. Recordings were carried out at −35 mV, 28 °C in 15 mM Tris·HCl pH 7.5 containing 150 mM NaCl. The I−V current traces were recorded with an automated voltage protocol that applied each potential for 0.4 s.

three ClyA types correspond to oligomers with a different stochiometry that offer different steric hindrance to HT.

Protein Interaction with ClyA Nanopores of Different Size. The ability to employ biological nanopores with identical amino acid composition but different size is important because the size of a nanopore defines its ability to capture and study a particular molecule.[22,52] The structure of the ClyA nanopores and the characteristics of HT induced current blockades suggest a physical model for the interaction of HT to Type I and Type II ClyA at −35 mV in which single folded protein molecules enter the pore from the cis side and are trapped for several minutes in the cis vestibule of ClyA (Figure 5a and SI Figure S3c). Most likely, the translocation to the trans side of the Type I and Type II ClyA-CS pores was prevented by the small diameter of the transmembrane region of Type I and Type II ClyA-CS (3.3 and 3.7 nm, respectively), which is smaller than the diameter of HT (~4.2 nm). To our surprise, in the voltage range from −90 to −150 mV, the duration of HT blockades to Type I and Type II ClyA-CS exponentially decreased with the applied potential (Figure 5b). The decrease of the duration of current blockades with increasing potential is often given as strong evidence to prove the translocation of an analyte molecule through a nanopore,[24,53−59] and suggests that HT might translocate through Type I and Type II ClyA in this voltage regime. Previous studies showed that proteins can be unfolded and translocated through small nanopores.[37,38,60] The voltage dependent translocation of those proteins occurred in a few seconds and was initiated by charged peptides or nucleic acids as leader sequences.[37,38,60] Therefore, the HT current blockades at high applied potentials might reflect folded HT lodging within the cis vestibule (additional discussion in SI), before the unfolding of C- or N- termini of HT under high-applied potential promotes the fast and undetected translocation of the protein through the pore. However, a complete unfolding of HT is unlikely because the HT structure is stabilized by four disulfide bridges and the trans diameter of the pore (3.3 nm in the 12mer ClyA nanopore) most likely does not require the complete unfolding of the protein to allow translocation. Therefore, it is possible that the applied potential and/or electroosmotic flow induce the deformation or partial unfolding of HT or the ClyA trans-membrane domain (additional discussion in the SI), thereby allowing HT to pass through the pore. Along these lines, a larger Type II ClyA-CS pore should provide a lower barrier to HT translocation

dx.doi.org/10.1021/ja4053398 | J. Am. Chem. Soc. 2013, 135, 13456−13463

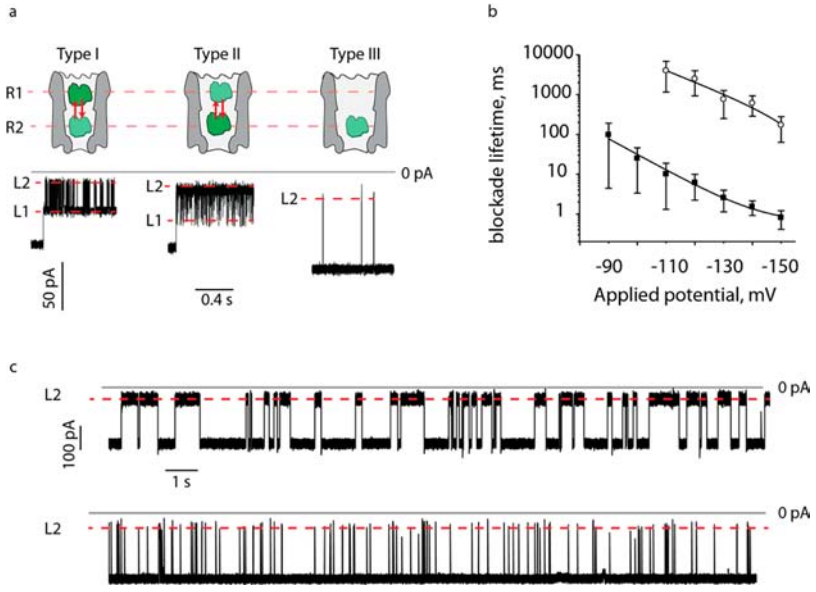

Figure 5. Current blockades provoked by HT to the different ClyA-CS nanopores types. (a) The cartoon representations (top) indicate the physical interpretation of the HT blockades (below) to Type I (left), Type II (middle) or Type III (right) ClyA-CS nanopores. HT current blockades to Type I and Type II ClyA-CS switched between L1 (I_{RES}% = 56 ± 1% and 68 ± 1%, respectively) and L2 (I_{RES}% = 23 ± 3% and 31 ± 1%, respectively) current levels, most likely corresponding to R1 and R2 residence sites within the ClyA structure. The blockades lasted for several minutes, therefore only the first second of the current traces is shown. In Type I ClyA-CS, L1 was the most represented current blockade (70%), while in Type II ClyA-CS L2 was mostly populated (96%). HT current blockades to Type III ClyA-CS nanopores only showed L2 current levels (I_{RES}% = 32 ± 9%). (b) Voltage dependency of HT blockade duration determined for Type I (hollow circles) and Type II (filled squares) ClyA-CS nanopores. The lines indicate single exponential fits to the experimental points. (c) HT current blockades to Type I (top) and Type II (bottom) ClyA-CS nanopores at −150 mV. The blockades showed only L2 current levels for both nanopores (I_{RES}% = 23 ± 1% and 29 ± 2%, for Type I and Type II ClyA-CS, respectively). The traces in (a) were collected applying a Bessel low-pass filter with 2000 Hz cutoff and sampled at 10 kHz. The traces in (c) were collected applying a Bessel low-pass filter with 10 kHz cutoff and sampled at 50 kHz in presence of 20 nM HT. All electrical recordings were carried out in 150 mM NaCl, 15 mM Tris·HCl pH 7.5 at 28 °C. Errors are given as standard deviations. The errors represent the standard deviation of the mean.

than Type I ClyA-CS, as manifested by ∼200 fold faster current blockades at −150 mV fixed applied potentials (Figure 5b, Table 1).

■ CONCLUSIONS

In this work, we used a directed evolution approach to obtain biological nanopores with desired properties. Evolved ClyA monomers showed high levels of soluble expression that allowed simple purification. In lipid bilayers, evolved ClyA oligomers showed uniform open pore conductance values and remained open in a wide range of applied potentials (e.g., +90 mV to −150 mV for Type I ClyA-CS). Remarkably, we could isolate three different nanopore types, which most likely correspond to the 12mer observed in the crystal structure,[42] the 13mer described in cryo-EM studies,[49] and a 14mer version of ClyA not observed before. Several lines of evidence support our interpretation: (i) The three nanopore types showed different electrophoretic motilities in blue native PAGE and, after gel extraction, reconstituted in planar lipid bilayers as nanopores with distinct conductance. (ii) The nanopore conductance of the three ClyA types compared well to the theoretical values calculated from the length and cross-section area of the 12mer, 13mer, and 14mer molecular models. (iii) The ionic current blockades of the HT model protein to the three ClyA pore types showed distinguishable current blockades and dwell times suggesting that larger pores imposed less steric hindrance to thrombin. Therefore, the three ClyA nanopore types provided a neat opportunity to sample proteins with nanopores of different diameter but identical chemical composition, and revealed that ∼10% variations in the diameter of nanopores are likely to greatly affect the recognition of a target protein analyte with the nanopore.

■ METHODS

Screening of ClyA Nanopores. As documented in detail in the SI, ClyA was expressed in *E. cloni* EXPRESS BL21 (DE3) cells (Lucigen) by using a pT7 plasmid. Transformants were prescreened on Brucella Agar with 5% Horse Blood (BBL, Becton, Dickinson and Company). Individual colonies were then grown and overexpressed in 96-deep-wells plates. Monomers from cell lysates were first screened for hemolytic activity on horse erythrocytes (bioMérieux) and then purified using Ni-NTA affinity chromatography. Purified monomers were oligomerized in the presence of 0.5% β-dodecyl maltoside (GLYCON Biochemicals GmbH)[49] and loaded on 4−20% blue native gel electrophoresis gels to check for oligomerization. The electrical properties of ClyA oligomers were then screened in planar lipid bilayers.

Purification of Evolved ClyA Nanopores. ClyA was expressed in *E. cloni* EXPRESS BL21 (DE3) cells using a pT7 plasmid. Monomers were purified by using Ni-NTA affinity chromatography and oligomerized in the presence of 0.5% β-dodecyl maltoside (GLYCON Biochemicals GmbH).

Electrical Recordings. Ionic currents were measured by recording from planar bilayers formed from diphytanoyl-*sn*-glycero-3-phosphocholine (Avanti Polar Lipids, Alabaster, AL). Currents were measured with Ag/AgCl electrodes by using a patch-clamp amplifier (Axopatch 200B, Axon Instruments, Foster City, CA) as previously described.[61]

dx.doi.org/10.1021/ja4053398 | J. Am. Chem. Soc. 2013, 135, 13456−13463

■ ASSOCIATED CONTENT

Supporting Information

Full documentation of material methods, additional discussion, and additional Tables and Figures. This material is available free of charge via the Internet at http://pubs.acs.org.

■ AUTHOR INFORMATION

Corresponding Author

giovanni.maglia@chem.kuleuven.be

Author Contributions

The manuscript was written through contributions of all authors.

Notes

The authors declare no competing financial interest.

■ ACKNOWLEDGMENTS

We thank the European Research Council (European Commission's Seventh Framework Programme, Project No. 260884) for funding. A.B. is funded by a Ph.D. grant from the Agency for Innovation by Science and Technology (IWT) Flanders.

■ REFERENCES

(1) Kasianowicz, J. J.; Brandin, E.; Branton, D.; Deamer, D. W. *Proc. Natl. Acad. Sci. U.S.A.* **1996**, *93*, 13770.

(2) Vercoutere, W.; Winters-Hilt, S.; Olsen, H.; Deamer, D.; Haussler, D.; Akeson, M. *Nat. Biotechnol.* **2001**, *19*, 248.

(3) Howorka, S.; Cheley, S.; Bayley, H. *Nat. Biotechnol.* **2001**, *19*, 636.

(4) Dekker, C. *Nat. Nanotechnol.* **2007**, *2*, 209.

(5) Li, J.; Stein, D.; McMullan, C.; Branton, D.; Aziz, M. J.; Golovchenko, J. A. *Nature* **2001**, *412*, 166.

(6) Li, W.; Bell, N. A.; Hernandez-Ainsa, S.; Thacker, V. V.; Thackray, A. M.; Bujdoso, R.; Keyser, U. F. *ACS Nano* **2013**, *7*, 4129.

(7) Wang, G.; Zhang, B.; Wayment, J. R.; Harris, J. M.; White, H. S. *J. Am. Chem. Soc.* **2006**, *128*, 7679.

(8) Wei, R.; Martin, T. G.; Rant, U.; Dietz, H. *Angew. Chem., Int. Ed.* **2012**, *51*, 4864.

(9) Bell, N. A.; Engst, C. R.; Ablay, M.; Divitini, G.; Ducati, C.; Liedl, T.; Keyser, U. F. *Nano Lett.* **2012**, *12*, 512.

(10) Langecker, M.; Arnaut, V.; Martin, T. G.; List, J.; Renner, S.; Mayer, M.; Dietz, H.; Simmel, F. C. *Science* **2012**, *338*, 932.

(11) Burns, J. R.; Stulz, E.; Howorka, S. *Nano Lett.* **2013**, *13* (6), 2351−2356.

(12) Hall, A. R.; Scott, A.; Rotem, D.; Mehta, K. K.; Bayley, H.; Dekker, C. *Nat. Nanotechnol.* **2010**, *5*, 874.

(13) Venkatesan, B. M.; Bashir, R. *Nat. Nanotechnol.* **2011**, *6*, 615.

(14) Jung, Y.; Bayley, H.; Movileanu, L. *J. Am. Chem. Soc.* **2006**, *128*, 15332.

(15) Heinz, C.; Engelhardt, H.; Niederweis, M. *J. Biol. Chem.* **2003**, *278*, 8678.

(16) Franceschini, L.; Mikhailova, E.; Bayley, H.; Maglia, G. *Chem. Commun. (Camb.)* **2012**, *48*, 1520.

(17) Maglia, M.; Henricus, M.; Wyss, R.; Li, Q.; Cheley, S.; Bayley, H. *Nano Lett.* **2009**, *9*, 3831.

(18) Jing, P.; Haque, F.; Vonderheide, A. P.; Montemagno, C.; Guo, P. *Mol. Biosyst.* **2010**, *6*, 1844.

(19) Pastoriza-Gallego, M.; Oukhaled, G.; Mathe, J.; Thiebot, B.; Betton, J. M.; Auvray, L. C.; Pelta, J. *FEBS Lett.* **2007**, *581*, 3371.

(20) Japrung, D.; Henricus, M.; Li, Q. H.; Maglia, G.; Bayley, H. *Biophys. J.* **2010**, *98*, 1856.

(21) Fologea, D.; Ledden, B.; McNabb, D. S.; Li, J. *Appl. Phys. Lett.* **2007**, *91*, 539011.

(22) Plesa, C.; Kowalczyk, S. W.; Zinsmeester, R.; Grosberg, A. Y.; Rabin, Y.; Dekker, C. *Nano Lett* **2013**, *13* (2), 658−663.

(23) Han, A.; Creus, M.; Schurmann, G.; Linder, V.; Ward, T. R.; de Rooij, N. F.; Staufer, U. *Anal. Chem.* **2008**, *80*, 4651.

(24) Stefureac, R. I.; Trivedi, D.; Marziali, A.; Lee, J. S. *J. Phys.: Condens. Matter* **2010**, *22*, 454133.

(25) Oukhaled, A.; Bacri, L.; Pastoriza-Gallego, M.; Betton, J. M.; Pelta, J. *ACS Chem. Biol.* **2012**, *7*, 1935.

(26) Firnkes, M.; Pedone, D.; Knezevic, J.; Doblinger, M.; Rant, U. *Nano Lett.* **2010**, *10*, 2162.

(27) Yusko, E. C.; Johnson, J. M.; Majd, S.; Prangkio, P.; Rollings, R. C.; Li, J.; Yang, J.; Mayer, M. *Nat. Nanotechnol.* **2011**, *6*, 253.

(28) Niedzwiecki, D. J.; Grazul, J.; Movileanu, L. *J. Am. Chem. Soc.* **2010**, *132*, 10816.

(29) Bikwemu, R.; Wolfe, A. J.; Xing, X.; Movileanu, L. *J. Phys.: Condens. Matter* **2010**, *22*, 454117.

(30) Wolfe, A. J.; Mohammad, M. M.; Cheley, S.; Bayley, H.; Movileanu, L. *J. Am. Chem. Soc.* **2007**, *129*, 14034.

(31) Movileanu, L.; Schmittschmitt, J. P.; Scholtz, J. M.; Bayley, H. *Biophys. J.* **2005**, *89*, 1030.

(32) Payet, L.; Martinho, M.; Pastoriza-Gallego, M.; Betton, J. M.; Auvray, L.; Pelta, J.; Mathe, J. *Anal. Chem.* **2012**, *84*, 4071.

(33) Pastoriza-Gallego, M.; Rabah, L.; Gibrat, G.; Thiebot, B.; van der Goot, F. G.; Auvray, L.; Betton, J. M.; Pelta, J. *J. Am. Chem. Soc.* **2011**, *133*, 2923.

(34) Oukhaled, G.; Mathé, J.; Biance, A.-L.; Bacri, L.; Betton, J.-M.; Lairez, D.; Pelta, J.; Auvray, L. *Phys. Rev. Lett.* **2007**, *98*, 158101.

(35) Stefureac, R. I.; Lee, J. S. *Small* **2008**, *4*, 1646.

(36) Stefureac, R.; Long, Y. T.; Kraatz, H. B.; Howard, P.; Lee, J. S. *Biochemistry* **2006**, *45*, 9172.

(37) Nivala, J.; Marks, D. B.; Akeson, M. *Nat. Biotechnol.* **2013**, *31*, 247.

(38) Rodriguez-Larrea, D.; Bayley, H. *Nat. Nanotechnol.* **2013**, *8*, 288.

(39) Wendell, D.; Jing, P.; Geng, J.; Subramaniam, V.; Lee, T. J.; Montemagno, C.; Guo, P. X. *Nat. Nanotechnol.* **2009**, *4*, 765.

(40) Mohammad, M. M.; Iyer, R.; Howard, K. R.; McPike, M. P.; Borer, P. N.; Movileanu, L. *J. Am. Chem. Soc.* **2012**, *134*, 9521.

(41) Soskine, M.; Biesemans, A.; Moeyaert, B.; Cheley, S.; Bayley, H.; Maglia, G. *Nano Lett.* **2012**, *12*, 4895.

(42) Mueller, M.; Grauschopf, U.; Maier, T.; Glockshuber, R.; Ban, N. *Nature* **2009**, *459*, 726.

(43) Wai, S. N.; Westermark, M.; Oscarsson, J.; Jass, J.; Maier, E.; Benz, R.; Uhlin, B. E. *J. Bacteriol.* **2003**, *185*, 5491.

(44) Pogoryelov, D.; Klyszejko, A. L.; Krasnoselska, G. O.; Heller, E. M.; Leone, V.; Langer, J. D.; Vonck, J.; Muller, D. J.; Faraldo-Gomez, J. D.; Meier, T. *Proc. Natl. Acad. Sci. U. S. A.* **2012**, *109*, E1599.

(45) Bayfield, O. W.; Chen, C. S.; Patterson, A. R.; Luan, W.; Smits, C.; Gollnick, P.; Antson, A. A. *PLoS One* **2012**, *7*, e44309.

(46) Lebedev, A. A.; Krause, M. H.; Isidro, A. L.; Vagin, A. A.; Orlova, E. V.; Turner, J.; Dodson, E. J.; Tavares, P.; Antson, A. A. *EMBO J.* **2007**, *26*, 1984.

(47) Geng, J.; Wang, S.; Fang, H.; Guo, P. *ACS Nano* **2013**, *7*, 3315.

(48) Tzokov, S. B.; Wyborn, N. R.; Stillman, T. J.; Jamieson, S.; Czudnochowski, N.; Artymiuk, P. J.; Green, J.; Bullough, P. A. *J. Biol. Chem.* **2006**, *281*, 23042.

(49) Eifler, N.; Vetsch, M.; Gregorini, M.; Ringler, P.; Chami, M.; Philippsen, A.; Fritz, A.; Muller, S. A.; Glockshuber, R.; Engel, A.; Grauschopf, U. *EMBO J.* **2006**, *25*, 2652.

(50) Kowalczyk, S. W.; Grosberg, A. Y.; Rabin, Y.; Dekker, C. *Nanotechnology* **2011**, *22*, 315101.

(51) McCleskey, R. B. *J. Chem. Eng. Data* **2011**, *56*, 317.

(52) Niedzwiecki, D. J.; Iyer, R.; Borer, P. N.; Movileanu, L. *ACS Nano* **2013**, *7* (4), 3341−3350.

(53) Clarke, J.; Wu, H.; Jayasinghe, L.; Patel, A.; Reid, S.; Bayley, H. *Nat. Nanotechnol.* **2009**, *4*, 265.

(54) Rincon-Restrepo, M.; Mikhailova, E.; Bayley, H.; Maglia, G. *Nano Lett.* **2011**, *11*, 746.

(55) Cracknell, J. A.; Japrung, D.; Bayley, H. *Nano Lett.* **2013**, *13* (6), 2500−2505.

(56) Maglia, G.; Rincon Restrepo, M.; Mikhailova, E.; Bayley, H. *Proc. Natl. Acad. Sci. U. S. A.* **2008**, *105*, 19720.

(57) Meller, A. *J. Phys.: Condens. Matter* **2003**, *15*, R581.
(58) Wanunu, M.; Sutin, J.; McNally, B.; Chow, A.; Meller, A. *Biophys. J.* **2008**, *95*, 4716.
(59) de Zoysa, R. S.; Krishantha, D. M.; Zhao, Q.; Gupta, J.; Guan, X. *Electrophoresis* **2011**, *32*, 3034.
(60) Thoren, K. L.; Worden, E. J.; Yassif, J. M.; Krantz, B. A. *Proc. Natl. Acad. Sci. U. S. A.* **2009**, *106*, 21555.
(61) Maglia, G.; Heron, A. J.; Stoddart, D.; Japrung, D.; Bayley, H. *Methods Enzymol., B* **2010**, *475*, 591.